Journal of Materials Chemistry B

Accepted Manuscript

ROYAL SOCIETY OF CHEMISTRY

www.rsc.org/materialsB

DOX-encapsulated intelligent PAA-*g*-PEG/PEG-Fa polymeric micelles for intensifying antitumoral therapeutic effect via active-targeted tumor accumulation

Yong Sun, Yaning Wang, Yani Cui, Wen Zou, Yanfei Tan, Jie Liang, Yujiang Fan*, Xingdong Zhang

National Engineering Research Center for Biomaterials, Sichuan University,

29 Wangjiang Road, Chengdu 610064, China

*Corresponding author to whom correspondence and proofs should be sent.

Yujiang Fan

National Engineering Research Center for Biomaterials, Sichuan University

29 Wangjiang Road, Chengdu 610064, China

Tel: +86-28-85416196

Fax: +86-28-85416196

E-mail: fan_yujiang@scu.edu.cn

Abstract

Stimuli-responsive targeted polymeric micelles as drug delivery systems have recently attracted significant attention for treatment of various cancers, which could improve delivery efficiency by tumor-specific recognition via active targeting strategies. In this research, DOX-incorporated bioreducible polymeric micelles based on PAA-*g*-PEG/PEG-Fa conjugated polymers were prepared and characterized as nanocarriers for promoting intracellular anti-tumor drug delivery efficiency via folate receptor-mediated endocytosis. The anti-proliferative activity on cancer cells, biodistribution, active-/passive-targeting efficiency, tumor growth inhibition efficiency, and biological toxicity were evaluated *in vitro* and *in vivo*. The MTT assay demostrated that the DOX-encapsulated active-targeting PAA-*g*-PEG/PEG-Fa micelles had much greater growth inhibition effect against 4T1 and KB than that of passive-targeting micelles. These active-targeting micelles showed superior tumor accumulation and excellent tumor growth inhibition effect as revealed by the fluorescence optical imaging technique and tumor volume change investigation, as well as survive study of the tumor-bearing Balb/c mice. Furthermore, the active targeting micelles greatly depressed the toxicity of DOX on the heart and other organs. These potential results encouraged us to further optimize the molecular structure to achieve more excellent targeted therapeutic effect.

Keywords: bioreducible micelles; active-targeting; folic acid; receptor-mediated; doxorubicin;

1、Introduction

In the past decades, tumor targeted therapies based on nano-drug carriers have been extensively investigated for improving treatment outcome, protecting the emergence of drug resistance, and reducing side effects.[1-4] An ideal anti-tumor drug carrier is prospected to have the following characteristics: long circulation time and intense stability in the bloodstream or in normal tissues, availably accumulating in tumor tissues by passive-/active-targeting, and smartly controlling the release of drugs in response to the local environment during cellular uptake by cancer cells.[5, 6] Polymeric micelles as drug delivery carriers have recently attracted significant attentions for targeted treatment of various cancers by loading hydrophobic anti-tumor drug, and exhibited a wide and promising future.[7, 8] Stimtli-responsive active-/passive-targeting polymeric micelles were formed by self-assembly of amphiphilic copolymers with hydrophobic inner core (which drives micelles formation in the water medium and keeps the micellar stability) and hydrophilic outer shell architecture (which regulates the nano-size of micelles and provides targeted characterization by chemical bonding targeted molecular or antibodies onto the surfaces of hydrophilic segment).[9-12] Adjustable chemical structure on either inner core or outer shell made these micelles sensitive to changes in extracellular and intracellular special signals, such as pH, temperature, light, magnetic, specific enzymes or redox conditions.[13-16]

Compared with passive-targeting polymeric micelles, the active-targeting polymeric micelles are a promising drug delivery systems for targeting cancer therapy, which could further improve the tumor-specificity recognition and the drug delivery efficiency via active-targeting strategies.[17-19] One of the most effective strategies involves coupling a specific ligand on the hydrophilic segment of polymeric micelles, which was recognizable by specific receptors overexpressed on the surface of cancer cells cytomembrane.[20-24] Folate receptor is a glycosylphosphatidylinositol-linked membrane glycoprotein of 38 kDa seated in caveolae, which is involved in the process of cellular accumulation of folate molecule via potocytosis mechanism.[25, 26] It is selectively overexpressed on the apical membrane

surface of certain epithelial cells, especially for brain, kidney, lung, and breast cancer cells. The overexpression of folate receptor on many cancer cells was distinctly conducive to employ folate as a potential targeting molecule for various ligand/antibody-directed cancer therapeutics to enhance the drug delivery efficiency through folate receptor-mediated endocytosis.[27-30] Therefore, the explosion of smart polymeric micelles conjugated with folate to target living cells has become an indispensable approach to improve their targeting ability by specific internalization of target cells.[31-34] Zhong et al reported that paclitaxel (PTX)-encapsulated folate-PEG-PLA (Fa-PEG-PLA) polymeric micelles could quickly enter the KB cells. This research showed us that ligand-conjugated PEG-PLA micelles have more efficient cellular uptake via folate receptor-mediated endocytosis, which possessed of a great potential in active-targeting tumor treatment.[35] In another report, Werner and his colleagues reported folate-targeted nanoparticles (PLGA-lecithin-PEG-Folate core-shell NPs) encapsulating Paclitaxel (PTX) for the treatment of ovarian cancer peritoneal metastasis. The *in vivo* studies results indicated that folate-targeted nanoparticles (NP) therapeutics were significantly more effective than non-targeted NP therapeutics, which have the potential as a treatment for ovarian peritoneal metastasis.[36] Recently, Huang and Li prepared doxorubicin-loaded folate modified HPMA polymeric micelles, which could enhance cytotoxicity, led to stronger apoptosis and greater tumor spheroid inhibition towards Hela cells.[37]

In our previous research,[38, 39] smart drug delivery systems were developed in which anti-tumor drug doxorubicin (DOX) was encapsulated in reduction-breakable amphiphilic polyethylene glycol-g-polyamide amine (PAA-*g*-PEG) polymeric micelles. Compared with the traditional drug release system[40, 41], the hydrophobic segments of PAA-*g*-PEG contained reductively cleavable disulfide bond and aromatic structure throughout the macromolecular chain, which strengthened the stability of micelles, suppressed immature drug release before the micelles reached the disease sites of interest, and resulted in intracellular breakdown of micelles under reductive condition in cancer cells and

quickly released the model drug. These passive-targeting polymeric micelles revealed high drug loading content and good passive targeting ability.

Depended on these research results, in this work, folate was chosen as the targeting molecule to conjugate on the surface of hydrophilic PEG segment to prepare polymeric micelles from amphiphilic polyamide amine-*g*-polyethylene glycol/polyethylene glycol conjugeted folate (PAA-*g*-PEG/PEG-Fa) copolymer to enhance targeting therapeutic effect. For further studying the influence of folate molecular on the characteristics and biological function of DOX-encapsulated PAA-*g*-PEG/PEG-Fa micelles, six kinds of active-targeting bioreducible micelles with different molecular compositions and drug contents were investigated *in vitro* and *in vivo*, and compared with the passive-targeting DOX-encapsulated PAA-*g*-PEG micelles. The characterization was carried out by UV, ^{1}H NMR, TEM and DLS, and the antiproliferative activity was investigated in cancer cell lines presenting the folic acid receptors. Besides, the biodistribution, targeted accumulation and active-/passive-targeting efficiency were visualized using *in vivo* imaging system in 4T1 tumor-bearing nude mice. Meanwhile, the tumor growth inhibition efficiency and the biological toxicity were also evaluated in 4T1 tumor-bearing Balb/c mice and normal Balb/c mice.

2、 Materials and methods

2.1 Materials and measurements

α-carboxy-ω-methoxy polyethylene glycol (MPEG-COOH, Mn 2000 and 5000) and α-carboxy-ω-amino polyethylene glycol (HOOC-PEG-NH_2, Mn 2000 and 4000) were purchased from Shanghai Yare Biotech, Inc. (Shanghai, China). Acryloyl chloride, phenethylamine, ethanolamine, and folic acid were obtained from Aladdin (Shanghai, China). Doxorubicin hydrochloride (DOX·HCl, >99%), triethylaminecystamine (TEA), dihydrochloride, N, N'-dicyclohexyl carbodiimide (DCC), dimethylamine pyridine (DMAP), and N-hydroxysuccinimide (NHS) were purchased from

AstaTech Biopharm. Co., Ltd. (Chengdu, China) and were used as-received. Dimethyl formamide (DMF) and dimethyl sulfoxide (DMSO) were chromatographically pure and were received from Sigma-Aldrich.

*2.2 Synthesis of PAA-g-PEG/*PEG-Fa *graft copolymer*

Six kinds of PAA-*g*-PEG/PEG-Fa graft copolymers with different proportion of PEG and PEG-Fa were synthesized as the following. Firstly, the hydrophobic PAA main backbone containing disulfide linkage (mol ratio: phenethylamine/ethanolamine = 8/2 and 7/3, respectively) was acquired according to the method reported previously.[39] Secondly, to prepare folate-CONH-PEG-COOH, folic acid was activated to get the folate-NHS under the catalysis of DCC (1.2 times) and NHS (1.2 times) in dry DMSO at room temperature. After removal of precipitated DCU by filtration, the equimolar quantities of α-carboxy-ω-amino polyethylene glycol (HOOC-PEG-NH_2, Mn 2000 or 4000) were added into the filtrate to obtain folate-CONH-PEG_{2000}-COOH and folate-CONH-PEG_{4000}-COOH in DMSO, respectively. Finally, as an example, reduction-degradable amphiphilic $PAA_{7:3}$-*g*-$2PEG_{2000}$/PEG_{2000}-Fa copolymer was obtained by coupling $MPEG_{2000}$-COOH and folate-CONH-PEG_{2000}-COOH (molar ratio 2:1) on PAA (phenethylamine/ethanolamine = 7/3, molar ratio, carboxy/hydroxyl = 1:1) using DCC as coupling agent and DMAP as catalyst in dry DMSO at room temperature. The raw product was re-precipitated in dry ethyl ether/ethyl acetate for 3 times, dialyzed (MWCO 14000) against pure water, and then freeze-dried to yield the $PAA_{7:3}$-*g*-$2PEG_{2000}$/PEG_{2000}-Fa copolymer. Following the above synthetic route (as show in scheme 1), six kinds of folate targeted compolymer were synthesised.

2.3 Fabrication, characterization and biocompatibility of the DOX-encapsulated micelles

DOX·HCl was stirred at room temperature with excess TEA (1.5×DOX·HCl) in DMSO overnight to obtain a DOX base fluid. 0.3 mL of DOX solution (10 mg/mL) was mixed with 0.2 mL DMSO solution containing 10 mg of freeze-dried PAA-*g*-PEG/PEG-Fa copolymer in a 2 mL glass vial, and stirred for 2h. The solution was added dropwise to deionized water (10 mL) within 10 min under

stirring. The mixture was then transferred into a dialysis tube (Spectra/Por, MWCO 14,000) and thoroughly dialyzed against deionized water at room temperature for 24 h with frequent change of water. The micelle suspension in the dialysis tube that fresh prepared was filtered through a 0.45 nm membrane filter (Millipore) to remove the DOX aggregates. Subsequently the mixture was ultrafiltered through a Millipore Centrifugal Filter Device (MWCO: 10,000) at 3500 r/min until the intraluminal fluid reached 3 mL to further remove unpacked free DOX and DMSO, and concentrate the DOX-encapsulated micelles suspension. The suspension was collected and kept at 4℃. The whole procedure was performed in dark.

The mean particle size and morphology of the micelles and DOX-encapsulated micelles were measured by transmission electronic microscopy (TEM, Hitachi H-600) and dynamic light scattering (DLS, Malvern Nano-ZS). The drug loading efficiency (DLE) and Drug loading content (DLC) were determined by ultraviolet spectrometry measurement (F-7000, excitation at 485 nm) in DMSO using calibration curve obtained from DOX/DMSO solutions with different DOX concentrations. The calculation formula of DLC and DLE were as follow:

DLC (wt%) = [weight of loaded drug/weight of drug-encapsulated micelle] × 100%

DLE (%) = [weight of loaded drug/weight of drug in feed] × 100%

The DOX *in vitro* release profiles of DOX-encapsulated micelles were investigated by dialysis the DOX-encapsulated PAA-*g*-PEG/PEG-Fa micelles suspension in PBS buffer (10 mM, pH 7.4) with different concentration of reductant DTT. Briefly, 2 mL of micelles suspension (1.88 mg of DOX-encapsulated micelles, DLC 21.3 wt%, containing 400 μg DOX) was dialyzed against 30 mL of PBS buffer (Spectra/Por, MWCO 14000) solutions contain different concentration of DTT (0, 1 and 10 mM). At predetermined time intervals, 10 mL media outside the dialysis tube were removed and replaced with fresh PBS buffer solution. DOX concentration was calculated based on the absorbance intensity at 485 nm using fluorescence measurement (F-7000). All procedures were performed in dark

and repeated three times.

The biocompatibility of the micellar carrier material was evaluated by co-culture the micelles with L929 cells. Briefly, L929 cells were seeded into 96-well plates at 5×10^3/well cell density in 100 μL DMEM culture medium supplemented with 10% fetal bovine serum and 1% benzylpenicillin/streptomycin at 37°C in a humidified atmosphere with 5% CO_2 for 12 h. Then the culture media were replaced by media containing different concentration of micelles (0, 10, 40, 100 and 250 μg/mL). After 48 h, the carrier solution was removed and the wells were rinsed with PBS. 200 μL PBS (10 mM, pH 7.4) contain 20 μL MTT solution (5 mg/mL) were then added to each well. After the cells were incubated for an additional 4 h, the medium containing unreacted MTT was removed carefully. 150 μL DMSO was added into each well to dissolve the formed blue formazan crystals, and the absorbance was measured in a Thermo Scientific Varioskan Flash at the wavelength of 490 nm.

2.4 *Cytotoxicity*

The cytotoxicity of the DOX-encapsulated micelles was also evaluated by MTT assay as mentioned above using 4T1 and KB cancer cells. 4T1 cells and KB cells were seeded into 96-well plates at 5×10^3 cell/well density, and incubated for 12 h. Then the culture medium was replaced with 100 μL of the freshly pre-prepared culture medium containing free DOX or drug loaded micelles with different equivalent DOX concentration (0.001, 0.01, 0.05, 0.1, 0.5, 1.0 and 10 μg/mL). After 48h, the cell viability was evaluated by MTT assay.

2.5 Animal experiments

All animal experiments were approved by the Sichuan Provincial Committee for Experimental Animal Management. Nude mice and Balb/c mice were supplied by the Experimental Animal Center in West China Medical School of Sichuan University, and bred in SPF class animal facility in a sterile environment with temperature of 20–22°C, relative humidity of 50–60% and 12 h light–dark cycles with access to commercial rat pellet diet and water ad libitum.

2.6 Tumor targeted aggregation and organ biodistribution of DOX in athymic nude mice

The tumor-bearing nude mice model were builded by injecting a suspension of 1×10^6 4T1 cells in 200 μL PBS (PH 7.4, 10 mM) into the subcutaneous dorsa of athymic nude mice (four weeks old, 16-20 g). After the tumor volume reached approximately 100 mm^3 (about 7 days), DOX-encapsulated micelles and free DOX were injected into the nude mice through tail vein injection at a dose of 10 mg/kg (DOX/body weight). The targeted aggregation and organs biodistribution of DOX in the live animals were observed by tracing the intrinsic fluorescence of DOX using an *in vivo* imaging system (Maestro Ex Pro, CRI, USA) at 1, 2 and 4 h after the injection. The excitation filters of *in vivo* imaging fluorescent signals were set in 490 nm to excite the DOX molecules. After completing the experiment in each interval time point, the nude mice were euthanized. The main organs (heart, liver, spleen, lung and kidney) and tumor were immediately took out to detect imaging signals of DOX. 5 wt% Chloral hydrate aqueous solution (7.5 mL/Kg, anaesthetic liquid/weight of mice) was used to anaesthetize the nude mice by intraperitoneal injection.

2.7 The anti-tumor effect of targeted DOX-encapsulated micelles against tumor-bearing Balb/c mice.

By subcutaneously injected 4T1 cells suspension (1×10^6 cells) in PBS (PH 7.4, 200 μl) in the backs of mice, 36 4T1 tumor-bearing Balb/c mice model (8 weeks of age, 20-25g male/female =1/1) were successfully built. When the tumor volume reached approximately 100 mm^3 (7 days after inoculation), animals were randomly divided into the following six treatment groups (n=6 per group, male/female=1/1): $PAA_{8:2}$-*g*-PEG_{5000} and $PAA_{8:2}$-*g*-PEG_{5000}/PEG_{4000}-Fa empty micelles, free doxorubicin (DOX·HCl), DOX-encapsulated $PAA_{8:2}$-*g*-PEG_{5000} and $PAA_{8:2}$-*g*-PEG_{5000}/PEG_{4000}-Fa micelles and PBS control groups. In each experiment group, DOX·HCl or DOX-encapsulated micelles solutions was injected via the lateral vein at 5mg/kg (DOX/bodyweight) dose. In empty micelle groups, the injection amount should be kept consistent in corresponding DOX-encapsulated micelles. All formulations were diluted with 0.9% sodium chloride. Animals were treated via the tail vein injection

at 3 different time points with an interval of 5 days (days 7, 13, and 19 after the 4T1 cells injection).

In order to observe the efficacy of treatment, we use the vernier caliper to measure the tumor size at an interval of 3 days. Meanwhile, the tumor volume (mm^3) was calculated using V= 0.5×(longest diameter)×(shortest diameter)^2, and the relative tumor volume was calculated as the ratio of tumor volume on that day to its initial value at the start of therapy to evaluate the anti-tumor effect. Mice body weight (as an indirect indicator of general animal wellness), clinical status, and mortality (for the life span study, the experiment was ended on day 53) were carefully recorded to further investigate anti-tumor effect.

At 23th day from cancer cells injection, two mice in each treatment group were sacrificed by cervical vertebra dislocation (male/female=1/1). The main organs (heart, liver, spleen, lung, and kidney) and tumor were harvested immediately, and were fixed in 10% formalin for 1 day at room temperature. The specimens were embedded in paraffin, sectioned along the longitudinal axis of the tissues, and then stained with hematoxylin and eosin (H&E). The pathological changes of tissues were observed using optical microscope.

2.8 The systematic toxicity of target DOX-loaded micelles against normal Balb/c *mice.*

30 healthy Balb/c mice (5 weeks of age, 16-20g per mouse, male/female =1/1) selected for biological toxicity evaluation were randomly divided into one control group and the following four treatment groups (n=6 mice per group, male/female=1/1): $PAA_{8:2}$-*g*-PEG_{5000}/PEG_{4000}-Fa empty micelles, free doxorubicin (DOX·HCl), Dox-encapsulated $PAA_{8:2}$-*g*-2PEG_{5000}/PEG_{4000}-Fa micelles. In each experiment group, DOX or DOX-encapsulated micelle solution (0.2 mL) was injected via the caudal vein at 5 mg/kg (DOX/body weight) dose. For micelles without drug, the injection amount was kept consistent in corresponding Dox-encapsulated micelles. All formulations were diluted with 0.9% sodium chloride. Animals were treated at 3 different time points with an interval of 5 days (days 0, 6, and 12). Changes of mice body weight (as an indirect indicator of general animal wellness) and clinical

status were carefully recorded. Histological analysis of main organs was carried out using the same processing method as mentioned above.

2.9 Statistical analysis

The statistical significance of differences between groups was determined using a student's t-test. P values<0.05 were considered significant, and significant differences are shown by asterisks in the figures.

3 Results and discussion

3.1 Fabrication, characterization and biocompatibility of PAA-g-PEG/PEG-Fa micelles

The reduction-sensitive $PAA_{8:2}$-*g*-PEG_{5000}/PEG_{4000}-Fa graft copolymer as a sample was synthesized in three steps as shown in Scheme 1. Firstly, the carboxyl group of folic acid (Fa-COOH) was preactivated to get the Fa-NHS under the catalysis of DCC (1.2 mmol) and NHS (1.2 mmol) in dry DMSO at room temperature for 6 h. Secondly, the equimolar quantities of α-carboxy-ω-amino polyethylene glycol (HOOC-PEG-NH_2, Mn=4000) were added into the Fa-NHS reaction solution and reacted in DMSO at room temperature for 24 h. After reaction, the mixed solution were filtrated and dialysized ((MWCO 3500) against the deionized water, A yellow powder of Fa-PEG_{4000}-COOH was obtained after freeze drying. Subsequently, the hydrophobic $PAA_{8:2}$ (1 mmol) with main backbone containing disulfide linkage (mol ratio: phenethylamine/ethanolamine = 8/2) and DMAP (0.2 mmol, as catalyst), which was acquired as the method previously reported,[39] was coupled with $MPEG_{5000}$-COOH (1 mmol) and Fa-CONH-PEG_{4000}-COOH (1 mmol) (molar ratio: 1/1) to gain raw $PAA_{8:2}$-*g*-PEG_{5000}/PEG_{4000}-Fa graft copolymer. The raw product was purified by precipitation with dry ethyl ether/ethyl acetate for three times, and then dialyzed (MWCO 14000) against pure water and freeze-dried to yield the yellow powder $PAA_{8:2}$-*g*-PEG_{5000}/PEG_{4000}-Fa copolymer. The ^{1}H NMR spectra of amphiphilic $PAA_{8:2}$-*g*-PEG_{5000}/PEG_{4000}-Fa, hydrophobic $PAA_{8:2}$, COOH-PEG_{4000}-Fa, NHS-Fa and Fa

have been shown in Figure S1 (Supporting Information). This spectra data results effectively illustrate that the amphiphilic copolymers containing folic acid molecules on the surface of hydrophilic PEG shell have been successfully prepared.

For further investigating the effect of folate density and the ratio between hydrophobic and hydrophilic segments on fabrication, characterization and therapeutic efficacy of the drug-loaded micelles, according to different feeding ratio (PAA-OH/PEG-COOH/Fa-PEG-COOH), six graft copolymers with different proportion of hydrophobic segments, hydrophilic segments and folate molecular content were synthesized as summarized in Table 1. The structure of these copolymers were confirmed by ^{1}H NMR (Figure S1). It can be found from the integrals of signals in ^{1}H NMR that the PEG grafting efficiency of PEG_{2000} or PEG_{2000}-Fa was almost qualitative, whereas PEG_{5000} or PEG_{4000}-Fa showed less grafting efficiency, probably due to the lower reactivity resulting from the higher molecular weight.

As shown in Table 1, six kinds of empty micelles and DOX-encapsulated micelles were fabricated by dialyzing against deionized water. The diameter of all the empty micelles/DOX-encapsulated micelles was less than 120 nm with narrow size distribution (PDI less than 0.3), which was suitable for EPR effect and targeting the cancer to achieve intra-cellular targeting delivery of drugs. The TEM measurement indicated the morphology of all the micelles was spherical, and the size by TEM measured was less than that of DLS measured, probably due to the dehydration in the process of TEM measurement (Figure 1-A). Meanwhile, the nano-size of the micelles greatly depended on the ratio between hydrophobic segment molecular weight (M_WO) and hydrophilic segment molecular weight (M_WH). When the MwH/MwO value varied from 0.99 to 1.49, the diameter of empty micelles gradually reduced to minimum value 35.7 nm, and mildly increased to 57.6 after the MwH/MwO value increased from 1.49 to 3.47. When the hydrophobic drug of DOX was encapsulated in hydrophobic core, it might function as a part of hydrophobic segment to disturb the balance of

hydrophobic/hydrophilic to cause the change of the size of micelles. When the MwH/MwO value was less than 1.49, the nano-size of DOX-encapsulated micelles was less than that of empty micelles. However, once the value was over 1.49, the diameter would rapidly rise to up to 120 nm. On the other hand, all the DOX-encapsulated micelles had high drug loading content (DLC) and drug loading efficiency (DLE). As previously reported[38, 39], π–π stacking between aromatic structure of DOX and phenyl of PAA in the micelle core provided tight incorporation and contributed for the high DLC and DLE.

The drug release behavior of DOX-encapsulated micelles was investigated in a reduction sensitive manner against PBS buffer solution (PH=7.4, 10 mM) without and with reductant DTT at 37 °C to simulate physiological and intracellular reducing conditions. The representative drug release results of $PAA_{8:2}$-*g*-PEG_{5000}/PEG_{4000}-Fa DOX-encapsulated micelles (DLC: 21.3%) was illustrated as shown in Figure 1-B. Under the condition of non-reductive DTT, only small amount of drug (less than 5% of total quantity) was released until 24 h. When a low level of reducing substance DTT (1 mM) was added, an obviously increased DOX release was observed, with more than 25% after 12 h. And then, the DTT concentration in solution was adjusted to higher concentration of 10 mM，which significantly accelerated the drug release compared with the that of at 1 mM concentrations: the DOX release quickly rose from 25% under 1 mM DTT in prior 12 h to 80% under 10 mM DTT in later 12 h. It could be well declared that the high concentration reductant benefited the DOX release. Increased DTT molecular could cleave S-S bonds of the copolymer backbone more easily and caused the breakdown of the micelles, which could then result in easier release of DOX encapsulated in the micelle core. This reduction-sensitive releasing behavior is of particular analogous in the tumor cell intracellular DOX delivery. It is expected that DOX-encapsulated micelles reached the tumor site by EPR effect and quickly internalized inside the cells by specific endocytosis mechanism due to the presence of folate, and rapidly release DOX due to the higher reducing agent glutamylcysteinylglycine (GSH)

concentration in cancer cell compared with that in normal cell (Scheme 2).

L929 fibroblasts were co-cultured with micelles (without encapsulation of DOX) at different concentration to evaluate the biocompatibility of the micelles. MTT assay in Figure 1-C showed that these micelles had good biocompatibility. Compared with blank control, $PAA_{8:2}$-*g*-PEG_{5000}/PEG_{4000}-Fa (as a sample) revealed low cytotoxicity with concentration ranging from 10 μg/mL to 250 μg/mL after 72 h co-culture with L929 fibroblasts, indicating commendable biocompatibility of the blank $PAA_{8:2}$-*g*-PEG_{5000}/PEG_{4000}-Fa micelles.

3.2 Cytotoxicity of DOX-encapsulated micelles against 4T1 and KB cancer cells

It's been widely reported that the folate receptor mediated targeting of Fa modified micelles could observably enhanced the growth inhibition effects against some cancer cells. Zhao and his colleagues[42] prepared the folate-modified poly(2-ethyl-2-oxazoline) polymeric micelles, the *in vitro and in vivo* study results clearly manifested that Fa modified micelles could increase the specific delivery to folate receptor-positive human HeLa, KB and MCF-7/ADR cells, while was not apparently increased for folate receptor-negative A549 cells under the condition of the same test. The Hsieh et al[43] researched the folate tethered star-shaped PEG-PCL micelles were greater endocytosis into KB and MCF-7 cancer cells than those of DOX-loaded micelles without the folate ligand via folate receptor-mediated endocytosis and caveolae/lipid-raft mediated endocytosis. Besides, Prabaharan and Gong's team[44] reported that H40–PLA-*b*-MPEG/PEG–Fa block copolymer could provide higher cytotoxicity against the 4T1 mouse mammary carcinoma by receptor-mediated endocytosis. Therefore, in this study, 4T1 (breast cancer cell) and KB (Oral epithelial carcinoma) were chosed to survey growth inhibition effects of DOX-encapsulated micelles ($PAA_{8:2}$-*g*-PEG_{5000}/PEG_{4000}-Fa, $PAA_{8:2}$-*g*-PEG_{5000}) and free Dox using the MTT assay. Compared with the untreated cancer cells (control), the results showed that the cell viability of both 4T1 and KB cancer cells observably decreased in the presence of DOX-encapsulated micelles and free DOX·HCl (Figure 2-A and 2-B). Importantly, the growth inhibition effect of

DOX-encapsulated $PAA_{8:2}$-*g*-PEG_{5000}/PEG_{4000}-Fa micelles was much greater than that of DOX-encapsulated $PAA_{8:2}$-*g*-PEG_{5000} micelles, especially in the case of KB cells, where the cytotoxicity of DOX-encapsulated $PAA_{8:2}$-*g*-PEG_{5000}/PEG_{4000}-Fa micelles was even slightly better than that of free DOX·HCl. The reason of this phenomenon was that the folate receptor-mediated endocytic uptake of the $PAA_{8:2}$-*g*-PEG_{5000}/PEG_{4000}-Fa micelle was conducive to fast formation of endosomes, and thus fast release of DOX under the high reductive GSH concentration in tumor cells.

In addition, the Zhou's group reported[45] that the conjugation efficiency of folate could influence the growth inhibition effects of DOX-encapsulated micelles against cancer cells. The Figure S2 (Supporting Information) indicated that the molecular structure of PAA-*g*-PEG/PEG-Fa, especially for the conjugation efficiency of folate (CEF), would influenced the growth inhibition effects of DOX-encapsulated micelles against KB (Oral epithelial carcinoma) cancer cells. The DOX-encapsulated $PAA_{8:2}$-*g*-PEG_{5000}/PEG_{4000}-Fa micelle (CEF: 63%) had the best antitumor effect than that of DOX-encapsulated $PAA_{7:3}$-*g*-PEG_{5000}/$2PEG_{4000}$-Fa (CEF: 65%) and $PAA_{7:3}$-*g*-$2PEG_{5000}$/ PEG_{4000}-Fa (CEF: 57%) micelles.

3.3 Targeted accumulation of DOX-encapsulated polymeric micelles in the nude mouse 4T1 tumor model

To track the *in vivo* fate of the DOX-encapsulated micelles, especially for the tumor passive-/active-targeting accumulation behavior in 4T1 tumor-bearing nude mice, the DOX-encapsulated ($PAA_{8:2}$-*g*-PEG_{5000}/PEG_{4000}-Fa, $PAA_{8:2}$-*g*-PEG_{5000}) micelles, and DOX·HCl were intravenously administrated into nude mice, and were clearly visualized by monitoring real-time fluorescence intensity in the whole body after different time period (1, 2 and 4 hours, respectively) based on the fluorescence optical imaging technique. As shown in Figure 3, compared with DOX·HCl treated mouse, the DOX-encapsulated micelles treated mouse owned much stronger fluorescent signals

at the tumor site than that in other tissues. Further, the DOX-encapsulated $PAA_{8:2}$-*g*-PEG_{5000}/PEG_{4000}-Fa and $PAA_{8:2}$-*g*-PEG_{2000}/PEG_{2000}-Fa micelles showed higher fluorescent intensity than DOX-encapsulated $PAA_{8:2}$-*g*-PEG_{5000} micelles. In addition, the DOX-encapsulated $PAA_{8:2}$-*g*-PEG_{2000}/PEG_{2000}-Fa micelles had the strongest fluorescent signals; the tumor site fluorescent intensity in this group showed no tendency of attenuation within the time range from 1 to 4 hours. On contrast, the fluorescent signals of DOX-encapsulated $PAA_{8:2}$-*g*-PEG_{5000}/PEG_{4000}-Fa and $PAA_{8:2}$-*g*-PEG_{5000} micelles maximized at 2 hour, and began to weaken after 4 hours, suggesting that the folate was easier to exposure to the outside of the micelles to bond to Fa-receptor with PEG_{2000}/PEG_{2000}-Fa as the hydrophilic shell than with PEG_{5000}/PEG_{4000}-Fa as the hydrophilic shell. These results indicated that the folate in the surface of the Fa-micelles could benefit helping the accumulation of loaded drugs at the tumor site through receptor-mediated endocytic uptake.

After completing the above experiments at each time point, the nude mice were executed, and then the main organs (heart, liver, spleen, lung and kidney) and the tumor were immediately dissected to detect imaging signals of DOX. Figure 4 revealed the distribution and accumulation of DOX in these major organs and tumor by visible fluorescence signals. The tumor accumulation of DOX in DOX·HCl treated mouse was rather weak, and the fluorescence signals quickly reduced with the time extending, and only very weak fluorescence was detected 4 h post-injection. Compared with DOX·HCl treated mouse, the DOX-encapsulated micelles treated mouse demonstrated remarkable fluorescence signals in tumor. Meanwhile, DOX-encapsulated $PAA_{8:2}$-*g*-PEG_{2000}/PEG_{2000}-Fa (812-Fa) micelles treated mouse shown obviously most potent tumor accumulation among these micelles treated groups, and the fluorescence signals held constant after injected via tail vein in 4 h. These results were in consistence with that observed in living fluorescence imaging as discussed above. The different tumor targeting ability between different micelles was attributed to hydrophilic segment molecule structure distinction between 812-Fa micelle and 814-Fa micelle. The folic molecules on 812-Fa

micelle surface were easier to get into the target cells than those on 814-Fa micelles, because the PEG-Fa segments in 812-Fa micelle were longer than other PEG segments on the surface; but on the contrary, in 814-Fa micelle, PEG_{5000} molecules may prevented the PEG_{4000}-Fa molecules from targeting the cancer cell, and weakened the targeted accumulation efficiency of 814-Fa micelle. These results taken together manifested that the DOX-encapsulated micelles with conjugating folic acid targeted molecules played a more prominent role in promoting tumor targeted treatment ability, and were promising to be a potential high effective targeted drug vehicles. However, it had to be noticed that, along with the tumor accumulation of 812-Fa micelle, the distribution of this micelles in some organs (heart, spleen, and lung) was also significant.

3.4 The DOX-encapsulated micelles inhibited the 4T1 tumor growth of Balb/c mice

The tumor growth inhibition test was performed from day 7 since subcutaneous injection of 4T1 cells suspension, and the data was analyzed as shown in Figure 5-A. The tumor-bearing Balb/c mice was respectively treated with PBS, empty $PAA_{8:2}$-*g*-PEG_{5000}/PEG_{4000}-Fa (814-Fa) and $PAA_{8:2}$-*g*-PEG_{5000} (825) micelles, DOX·HCl, and DOX-encapsulated $PAA_{8:2}$-*g*-PEG_{5000}/PEG_{4000}-Fa (814-Fa) and $PAA_{8:2}$-*g*-PEG_{5000} (825) micelles through the tail vein injection at 3 different time points with an interval of 5 days (at day 7, 13, and 20) to evaluate the *in vivo* anti-tumor effect. Compared with the control groups (PBS and two kinds of empty micelles treated groups), DOX·HCl treated group shown statistically significant slowdown of tumor growth, indicating the pesticide effect of DOX· HCl as a well-known anti-cancer drug. In addition, DOX-encapsulated micelles treated groups (passive-targeting 825 micelle and active-targeting 814-Fa micelle) manifested further effective tumor inhibition ability through the statistically significant tumor volume reduction. These results consistently matched the prior reports.[39] By comparing the tumor growth inhibition results between passive-targeting 825 micelle and active-targeting 814-Fa micelle, it could be found that the active-targeting 814-Fa micelle treated group showed significant variation of tumor diameter. Namely,

active-targeting 814-Fa micelle had obviously stronger anti-tumor effect than that of passive-targeting 825 micelle, and greatly improved therapeutic efficiency of the micellar delivery system by EPR effect and active-targeting mechanism.

The body weight change of mice was also an important indicator for investigating the treatment effect. As shown in Figure 5-B, the information illustrated that the body weight of control groups (PBS and empty micelles) mice generally kept relatively constant compared with the initial value. The body weight in DOX-encapsulated micelles treated groups (passive- and active-targeting micelles) only slightly reduced about 5% after the treatment. However, it is worthy to note that the body weight of the DOX·HCl treated group decreased rapidly about 20% despite an exponential growth in tumor volume in the back of the mice. Those phenomena indicated that DOX·HCl brought out significant side effects on causing weight loss, but the encapsulation of DOX in the passive or active targeting micelles could effectively reduce the undesirable toxicities.

In addition, the average survival span of PBS, empty 814-Fa and 825 micelles, DOX·HCl, and DOX-encapsulated 814-Fa and 825 micelles treated mice were recorded to further study the anti-tumor effect. All mice in PBS and empty micelles treated groups died within 30 days. Figure 5-C showed that the value of average survival time is 26.0, 25.8, and 25.0 days for PBS, empty 814-Fa and 825 micelles treated mice, respectively. DOX·HCl treatment extended average life span to 28.5 days, and the longest survival time reached 32 days. On the other hand, DOX-encapsulated micelles (814-Fa and 825) treated groups demonstrated an remarkable increase in average survival time, which were expanded to 38.3 days and 45.0 days, respectively. Meanwhile, the longest survival time of the mice treated with 814-Fa micelles (53 days) was much longer than that of 825 treated mice (47 days), which sufficiently demonstrated that the active targeting micelles effectively enhanced the drug therapeutic effect, showed more excellent anti-tumor ability than passive targeting micelles, and prolonged the span of life of tumor-bearing mice.

In order to evaluate the influence of drugs on different organs, the main organs were dissected and sections were stained with hematoxylin and eosin (H&E) for histological analysis using untreated normal Balb/C mice as blank control (Figure 6). Compared with the blank group, all the main organs of tumor-bearing mice in PBS and empty micelles treated groups showed damages at different degree, which probably attributed to the wild growth and metastasis of cancer cells. In the drug treated groups, the free DOX·HCl treated mice developed significant damage in heart and spleen. The muscle fibers in cardiac tissues showed critical pathological changes and necrosis； the spleen striation lost and became complete fragmentation. However, in the DOX-encapsulated micelles treated mice, the tissue in heart, liver, and spleen had only slight pathological changes compared to the blank control groups despite significant DOX accumulation in these tissues in *in vivo* imaging results, indicating depressed toxicity of DOX on the heart and liver. The morphology of spleen appeared mild hypertrophy because of the growing solid tumor, and diseased tissues structure could be observed in lung and kidney, but the degree was much moderate compared to the DOX·HCl treated group. The probable reason for the improved therapeutic effect and weakened side effect of the DOX-encapsulated micelles could be ascribed to the passive-/active- targeting performance and reduction responsive release behavior of the micelles. Although the DOX-encapsulated active targeting micelles increased the drug accumulation in both the tumor and other organs, the low intracellular concentration of reductant GSH in normal cells did not triggered the release of DOX, whereas in tumor cells, high concentration of GSH could rapidly promote DOX release and heighten the bioavailability of the drugs.

3.5 Systemic toxicity of DOX-encapsulated micelles in normal mice

To further evaluate the *in vivo* biosecurity of the nanoparticular drug delivery system, the normal mice were chosen for toxicity study as previous reported.[39] The body weight change and clinical manifestations as important indicator of toxicity studies were investigated by intravenously injecting empty 814-Fa micelle, DOX·HCl, and DOX-encapsulated 814-Fa micelle. The body weight of all the

treated groups increased with different degree after 15 days (Figure 7). The relative growth of the body weight approximately reached 27.6%, 25.5%, and 20.4% for blank control, empty micelles, and DOX-encapsulated micelles treated mice, respectively. Despite the less growth of body weight in the empty micelles and DOX-encapsulated micelles treated mice, there were no statistically significant difference between the treated groups and blank control group. The slight toxicity shown in the empty micelle treated group might be resulted from the stimulation reaction of the injection process to the mice body. On the other hand, DOX·HCl caused significantly less growth of body weight, reached only 7.2% growth in 15 days, demonstrating its significant systemic toxicity. In addition, injection of DOX·HCl also caused physical weakness of mice, such as the loss of hair luster, loss of appetite, loss of vitality, and other correlative symptoms. After the injection of DOX-encapsulated 814-Fa micelle, the growth of mice was close to the empty micelle treated group, obviously higher than that of DOX·HCl treated ones.

Figure 8 showed the histological analyses of main organs (heart, liver, spleen, lung and kidney) after the mice were treated with PBS (Blank), empty micelles, DOX·HCl, and DOX-encapsulated micelles. No significant signal of damage appeared in DOX-encapsulated micelles treated groups. However, obviously damaged pathology of organs appeared in DOX·HCl treated group. Compared with the normal blank mice group, obvious organ fragmentation and pathological changes emerged from heart and spleen tissues. Such result further illustrated that the DOX·HCl showed significant side effects to mice major organs, especially for heart and spleen, but encapsulation of DOX in 814-Fa micelle could reduce drug toxicity and improve drug efficacy.

4 Conclusion

Six kinds of active targeting bioreducible polymeric micelles were synthesized and characterized as useful carriers for promoting the intracellular delivery of anti-tumor drug DOX by conjugating folate

on the surface of reducible PAA-*g*-PEG micelles as targeting moieties. These active-targeting micelles showed much greater growth inhibition effect against 4T1 and KB than that of passive-targeting micelles by MTT assay. In *in vivo* studies on nude mice breast carcinoma subcutaneous model, revealed that the DOX-encapsulated PAA-*g*-PEG/PEG-Fa micelles showed superior active-targeted accumulation ability on tumor site by the fluorescence optical imaging technique, and excellent solid tumor growth inhibition effect by investigating the change of tumor volume, as well as survive study of the tumor-bearing Balb/c mice. Meanwhile, DOX-encapsulated PAA-*g*-PEG/PEG-Fa micelles greatly depressed the toxicity of DOX on heart and other organs compared with DOX·HCl and passive-targeting PAA-*g*-PEG micelles, as revealed by systemic toxicity investigation in tumor bearing and normal mice. These potential results encouraged us to further optimize the molecular structure to achieve more excellent targeted therapeutic effect.

Acknowledgement

This work was sponsored by National Natural Science Foundation of China (Grant No. 21174090, 51403138) and Young Teachers Science Foundation of Sichuan University (Grant No. 2014SCU11016).

References

1. K. Bourzac, *Nature*, 2012, 491, S58-S60.
2. K. Cho, X. Wang, S. M. Nie, Z. Chen and D. M. Shin, *Clin. Cancer Res.*, 2008, 14, 1310-1316.
3. P. Parhi, C. Mohanty and S. K. Sahoo, *Drug Discov. Today*, 2012, 17, 1044-1052.
4. T. Lammers, F. Kiessling, W. E. Hennink and G. Storm, *J. Control. Release*, 2012, 161, 175-187.
5. N. Yabbarov, G. Posypanova, E. Vorontsov, S. Obydenny and E. Severin, *J. Control. Release*, 2013, 168, 135-141.
6. V. Torchilin, *Adv. Drug Delive. Rev.*, 2011, 63, 131-135.
7. D. Peer, J. M. Karp, S. Hong, O. C. Farokhzad, R. Margalit and R. Langer, *Nature*

nanotechnol., 2007, 2, 751-760.
8. P. FeiáGao, L. LingáZheng, L. JiaoáLiang, X. XiáYang, Y. FangáLi and C. ZhiáHuang, *J. Mater. Chem. B*, 2013, 1, 3202-3208.
9. A. Rösler, G. W. Vandermeulen and H.-A. Klok, *Adv. Drug Delive. Rev.*, 2012, 64, 270-279.
10. L. Brannon-Peppas and J. O. Blanchette, *Adv. Drug Delive. Rev.*, 2012, 64, 206-212.
11. Y. Wang and S. M. Grayson, *Adv. Drug Delive. Rev.*, 2012, 64, 852-865.
12. X. J. Yang, Q. Q. Xiao, C. X. Niu, N. Jin, J. Ouyang, X. Y. Xiao and D. C. He, *J. Mater. Chem. B*, 2013, 1, 2757-2763.
13. R. Cheng, F. Feng, F. H. Meng, C. Deng, J. Feijen and Z. Y. Zhong, *J. Control. Release*, 2011, 152, 2-12.
14. T. Gonzalo, G. Lollo, M. Garcia-Fuentes, D. Torres, J. Correa, R. Riguera, E. Fernandez-Megia, P. Calvo, P. Avilés and M. J. Guillén, *J. Control. Release*, 2013, 169, 10-16.
15. X. X. Ma, H. Q. Tao, K. Yang, L. Z. Feng, L. Cheng, X. Z. Shi, Y. G. Li, L. Guo and Z. Liu, *Nano Res.*, 2012, 5, 199-212.
16. Z. L. Cheng, A. Al Zaki, J. Z. Hui, V. R. Muzykantov and A. Tsourkas, *Science*, 2012, 338, 903-910.
17. L. M. Pan, Q. J. He, J. N. Liu, Y. Chen, M. Ma, L. L. Zhang and J. L. Shi, *J. Am. Chem. Soc.*, 2012, 134, 5722-5725.
18. H. N. He, J. X. Ye, Y. S. Wang, Q. Liu, H. S. Chung, Y. M. Kwon, M. C. Shin, K. Lee and V. C. Yang, *J. Control. Release*, 2014, 176, 123-132.
19. M. Z. Fahmi and J. Y. Chang, *RSC Adv.*, 2014, 4, 56713-56721.
20. E. J. Mostad and J. R. Prohaska, *Exp. Biol. Med.*, 2011, 236, 298-308.
21. J. L. Goldstein, R. G. Anderson and M. S. Brown, *Nature*, 1979, 279, 679-685.
22. M. R. Huo, A. F. Zou, C. L. Yao, Y. Zhang, J. P. Zhou, J. Wang, Q. N. Zhu, J. Li and Q. Zhang, *Biomaterials*, 2012, 33, 6^{39}3-6407.
23. J. X. Niu, A. D. Wang, Z. C. Ke and Z. B. Zheng, *J. Drug Target.*, 2014, 22, 712-723.
24. H. N. Li, Y. N. Cui, J. Liu, S. Q. Bian, J. Liang, Y. J. Fan and X. D. Zhang, *J. Mater. Chem. B*, 2014, 2, 3500-3510.
25. K. G. Rothberg, Y. Ying, J. F. Kolhouse, B. A. Kamen and R. Anderson, *J. Cell Biol.*, 1990, 110, 637-649.
26. J. Fan, N. Kureshy, K. S. Vitols and F. M. Huennekens, *Oncol. Res.*, 1994, 7, 511-516.
27. S. S. Wang, R. J. Lee, C. J. Mathias, M. A. Green and P. S. Low, *Bioconjugate chem.*, 1996, 7, 56-62.
28. H. Shmeeda, L. Mak, D. Tzemach, P. Astrahan, M. Tarshish and A. Gabizon, *Mol. Cancer Ther.*, 2006, 5, 818-824.
29. I. G. Campbell, T. A. Jones, W. D. Foulkes and J. Trowsdale, *Cancer Res.*, 1991, 51, 5329-5338.
30. S. D. Weitman, R. H. Lark, L. R. Coney, D. W. Fort, V. Frasca, V. R. Zurawski and B. A. Kamen, *Cancer Res.*, 1992, 52, 3396-3401.
31. Y. J. Lu and P. S. Low, *Adv. Drug Delive. Rev.*, 2012, 64, 342-352.
32. N. V. Cuong, Y. L. Li and M. F. Hsieh, *J. Mater. Chem.*, 2012, 22, 1006-1020.
33. H. M. Lin, H. Y. Lin and M. H. Chan, *J. Mater. Chem. B*, 2013, 1, 6147-6156.
34. G. Zhang, M. Zhang, J. He and P. Ni, *Polym. Chem.*, 2013, 4, 4515-4525.
35. J. Xiong, F. H. Meng, C. Wang, R. Cheng, Z. Liu and Z. Y. Zhong, *J. Mater. Chem.*, 2011, 21, 5786-5794.
36. M. E. Werner, S. Karve, R. Sukumar, N. D. Cummings, J. A. Copp, R. C. Chen, T. Zhang and A. Z. Wang, *Biomaterials*, 2011, 32, 8548-8554.
37. L. Li, K. M. Huh, Y. K. Lee and S. Y. Kim, *J. Mater. Chem.*, 2011, 21, 15288-15297.

38. Y. Sun, X. L. Yan, T. M. Yuan, J. Liang, Y. J. Fan, Z. W. Gu and X. D. Zhang, *Biomaterials*, 2010, 31, 7124-7131.
39. Y. Sun, W. Zou, S. Q. Bian, Y. H. Huang, Y. F. Tan, J. Liang, Y. J. Fan and X. D. Zhang, *Biomaterials*, 2013, 34, 6818-6828.
40. A. Gueerry, S. Cottaz, E. Fleury, J. Bernard and S. Halila, *Carbohyd. Polym.*, 2014, 112, 746-752.
41. Y. X. Wang, X. G. Zhang, P. E. Yu and C. X. Li, *Inter. J. Pharm.*, 2013, 441, 170-180.
42. L. Y. Qiu, L. Zhang, Y. M. Jin and Q. H. Zhao, *Inter. J. Pharm.*, 2013, 456, 315-324.
43. Y. L. Li, N. V. Cuong and M. F. Hsieh, *Polymers*, 2014, 6, 634-650.
44. M. Prabaharan, J. J. Grailer, S. Pilla, D. A. Steeber and S. Q. Gong, *Biomaterials*, 2009, 30, 3009-3019.
45. Z. M. Tang, D. Li, H. L. Sun, X. P. Chen and S. B. Zhou, *Biomaterials*, 2014, 35, 8015-8027.

Scheme and figure captions

Scheme 1. Synthetic scheme of amphiphilic reduction-degradable polyamide amine-g-polyethylene glycol/polyethylene glycol conjugeted folate graft copolymer.

Scheme 2. Illustration of intelligent PAA-g-PEG/PEG-Fa polymeric micelles intensifying antitumoral therapeutic effect delivery through EPR effect and via via active-targeting folate receptor-mediated endocytosis.

Figure 1. A: The particle size of empty and Dox-incorporated $PAA_{8:2}$-*g*-PEG_{5000}/PEG_{4000}-Fa micelles by DLS and TEM; B: *In vitro* Dox-release profiles of Dox-incorporated $PAA_{8:2}$-*g*-PEG_{5000}/PEG_{4000}-Fa micelle without or with reductant DTT; C: Biocompatibility assay of PAA8:2-g-PEG5000/PEG4000-Fa empty micelle in L929 cell after incubation for 3 days. The standard deviation for each data point was averaged over five samples (n = 5).

Figure 2. Cytotoxicity study of Dox-incorporated $PAA_{8:2}$-*g*-PEG_{5000}/PEG_{4000}-Fa micelle and free DOX in KB cell after incubation for 3 days (A) and 4T1 after incubation for 2 days (B). The standard deviation for each data point was averaged over five samples (n = 5).

Figure 3. *In vivo* optical fluorescence imaging of 4T1 tumor-bearing nude mice administrated with DOX·HCl, Dox-incorporated $PAA_{8:2}$-*g*-PEG_{5000} micelle (825/Dox), $PAA_{8:2}$-*g*-PEG_{5000}/PEG_{4000}-Fa (814-Fa/Dox) and $PAA_{8:2}$-*g*-PEG_{2000}/PEG_{2000}-Fa (812-Fa/Dox) micelles at 1, 2, 3, 4 h post-injection with 10 mg/kg of DOX equivalent dosage. Red circle specifies the location of tumor. The color indicates the relative fluorescence intensity.

Figure 4. Optical fluorescence imaging of major organs and tumor taken from tumor-bearing nude mice after 1, 2, 3, and 4 h post-injection of DOX·HCl, Dox-incorporated $PAA_{8:2}$-*g*-PEG_{5000} micelle (825/Dox), $PAA_{8:2}$-*g*-PEG_{5000}/PEG_{4000}-Fa (814-Fa/Dox) and $PAA_{8:2}$-*g*-PEG_{2000}/PEG_{2000}-Fa (812-Fa/Dox) micelles (10 mg/kg body weight of DOX equivalent dosage). The color indicates the relative fluorescence intensity.

Figure 5. A: The changes of relative tumor volume after subcutaneous injection B: The relative body weight changes of tumor-bearing Balb/C mice after intravenous injection (male/female=1/1, n=6); C: The survival curve of tumor-bearing Balb/C mice (male/female=1/1, n=4). The tumor-bearing Balb/C mice were treated with PBS (pH 7.4, as control), empty $PAA_{8:2}$-*g*-PEG_{5000} and $PAA_{8:2}$-*g*-PEG_{5000}/PEG_{4000}-Fa micelles, Dox-incorporated $PAA_{8:2}$-*g*-PEG_{5000} and $PAA_{8:2}$-*g*-PEG_{5000}/PEG_{4000}-Fa micelle, and DOX·HCl in tumor-bearing Balb/C mice. Each formula was intravenously administered three times at a five-day interval at a dose of 5 mg/kg of DOX equivalent. Data were presented as mean ± SD, * $p < 0.05$. (male/female=1/1, n=6).

Figure 6. Histological observation of major organs harvested from normal mouse (blank) and tumor-bearing mice treated with PBS (pH 7.4), empty $PAA_{8:2}$-*g*-PEG_{5000} and $PAA_{8:2}$-*g*-PEG_{5000}/PEG_{4000}-Fa micelles, DOX·HCl, Dox-incorporated $PAA_{8:2}$-*g*-PEG_{5000} and $PAA_{8:2}$-*g*-PEG_{5000}/PEG_{4000}-Fa micelles. The organs were harvested 16 days after intravenous injection of each formula. Histological analysis was conducted after H&E staining. Scale bar = 100 μm.

Figure 7. The relative body weight changes of normal Balb/C mice after intravenous injection with PBS (pH 7.4), empty $PAA_{8:2}$-*g*-PEG_{5000}/PEG_{4000}-Fa micelle, Dox-incorporated $PAA_{8:2}$-*g*-PEG_{5000}/PEG_{4000}-Fa micelle and DOX·HCl. Each formula was intravenously administered three times at a five-day interval at a dose of 5 mg/kg body weight. Data were presented as mean ± SD, *$p < 0.05$. (male/female=1/1, n=6).

Figure 8. Histological observation of major organs harvested from normal mouse treated with Blank, empty $PAA_{8:2}$-*g*-PEG_{5000}/PEG_{4000}-Fa micelle, Dox-incorporated $PAA_{8:2}$-*g*-PEG_{5000}/PEG_{4000}-Fa micelle and DOX·HCl. The organs were harvested 16 days after intravenous injection of each formula. Histological analysis was conducted after H&E staining. Scale bar = 100 μm.

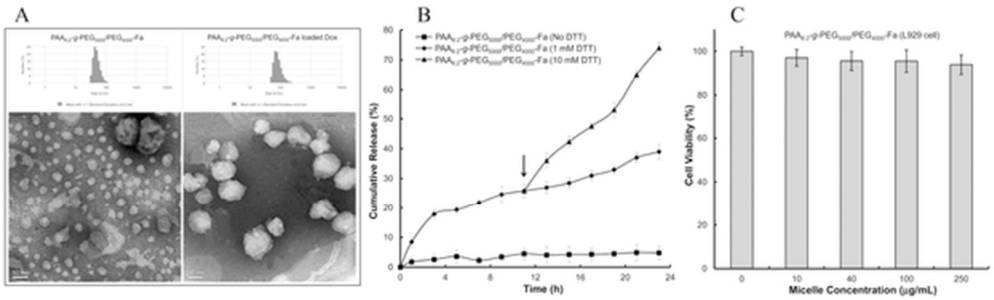

Figure 1
53x16mm (300 x 300 DPI)

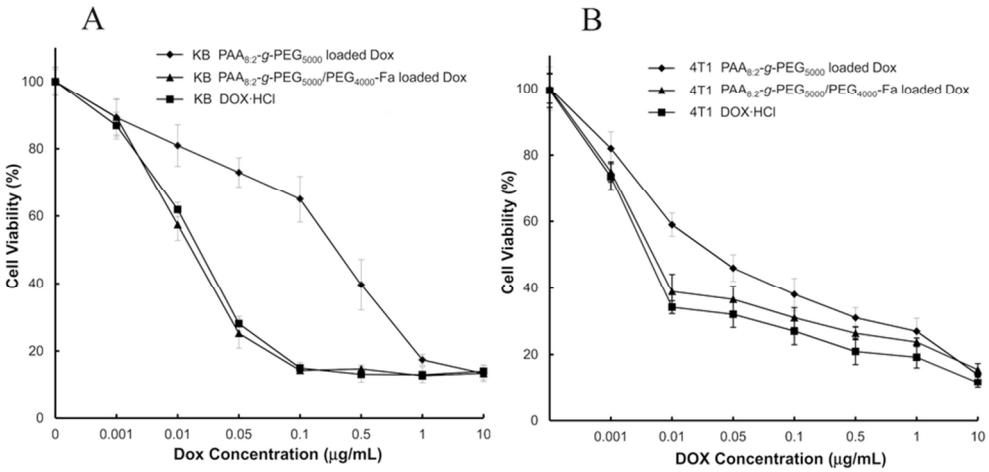

Figure 2
82x40mm (300 x 300 DPI)

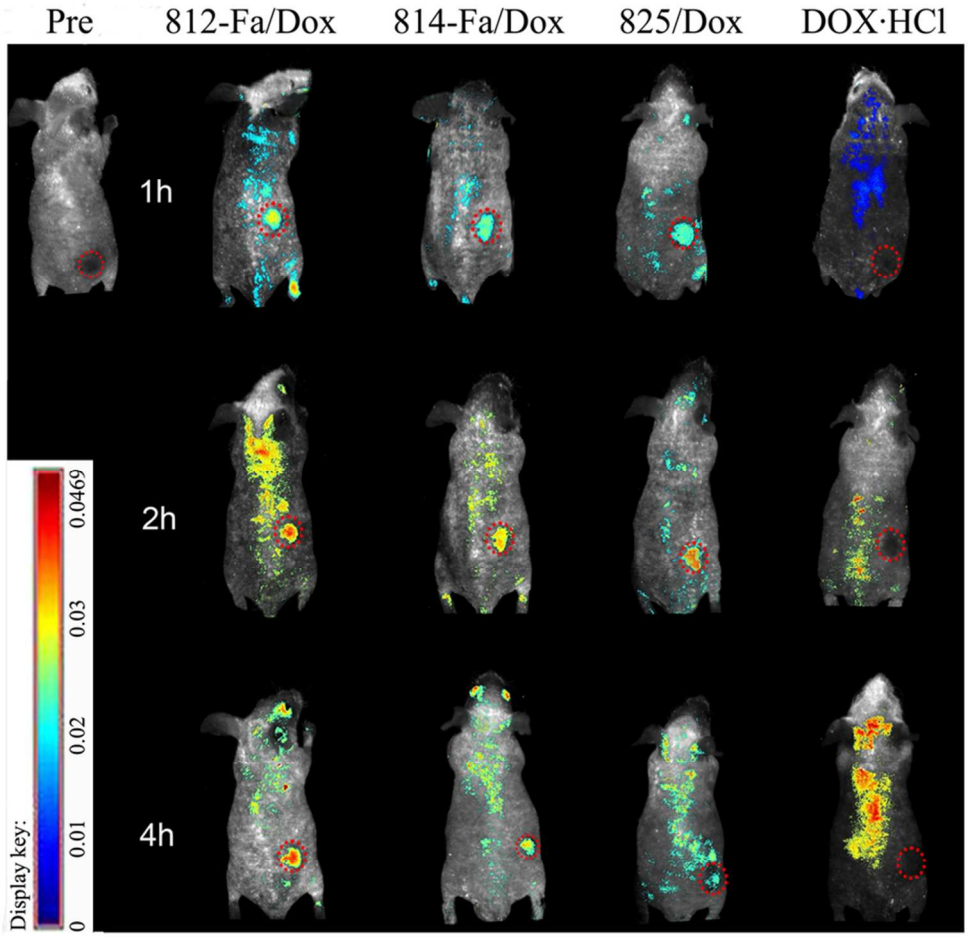

Figure 3
80x78mm (300 x 300 DPI)

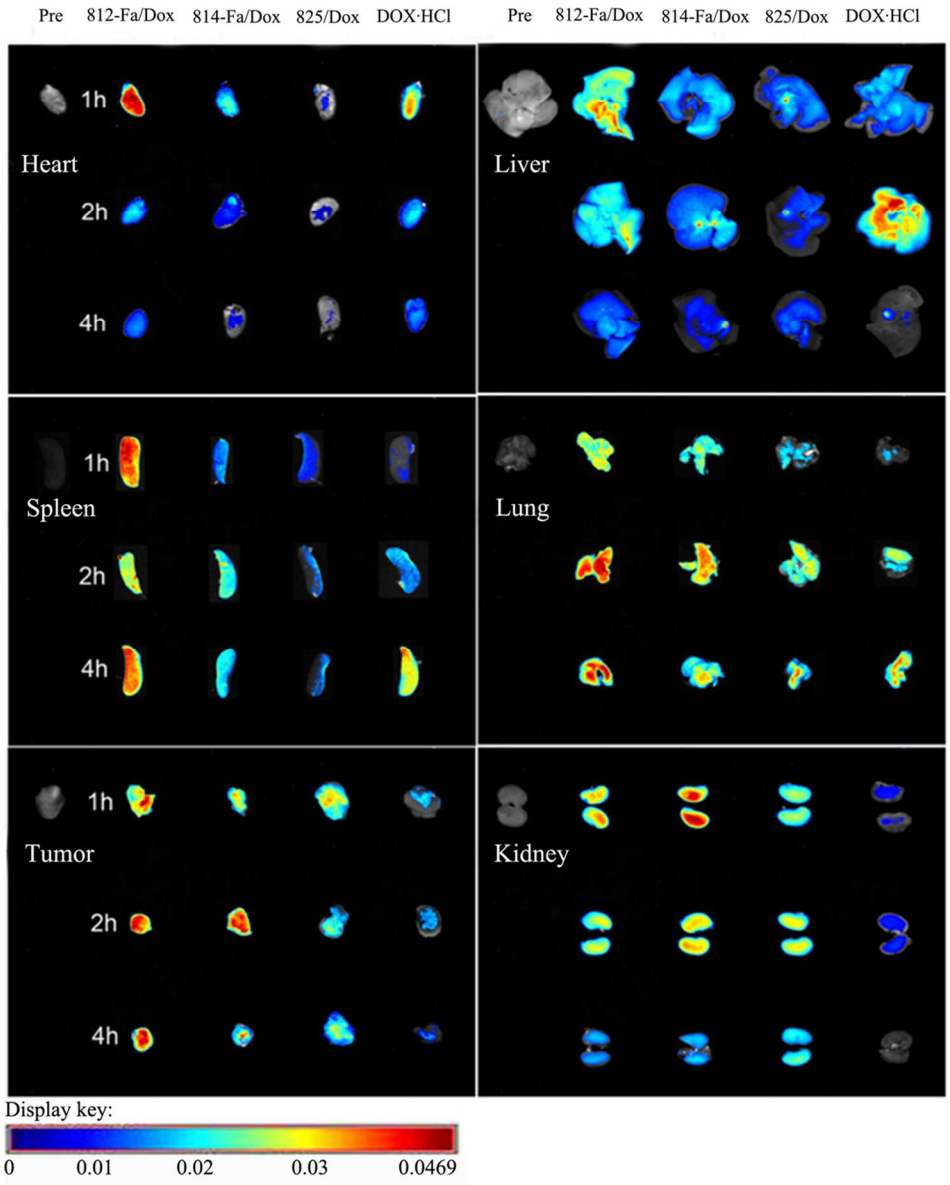

Figure 4
101x125mm (300 x 300 DPI)

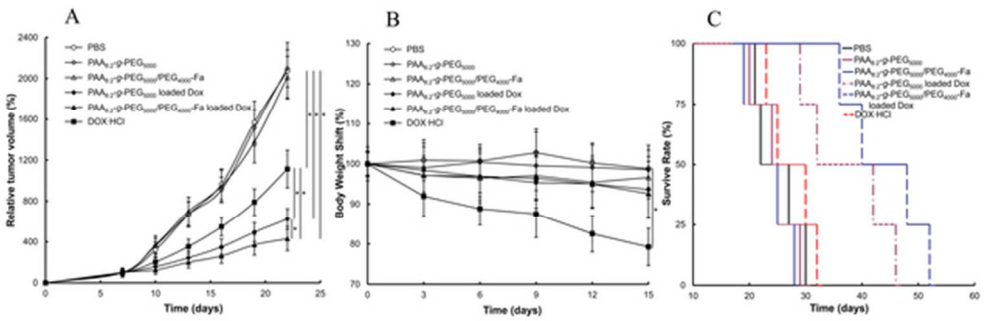

Figure 5
54x17mm (300 x 300 DPI)

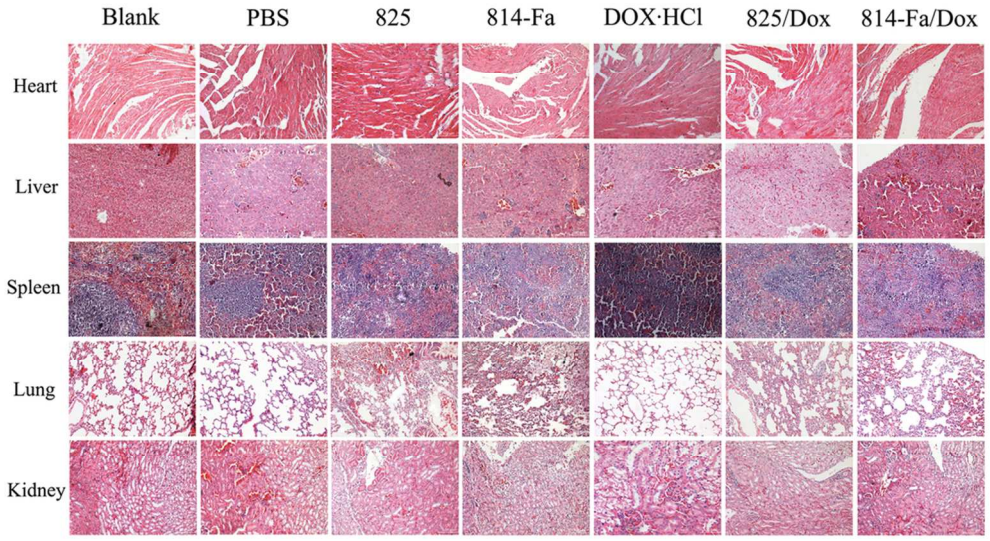

Figure 6
98x56mm (300 x 300 DPI)

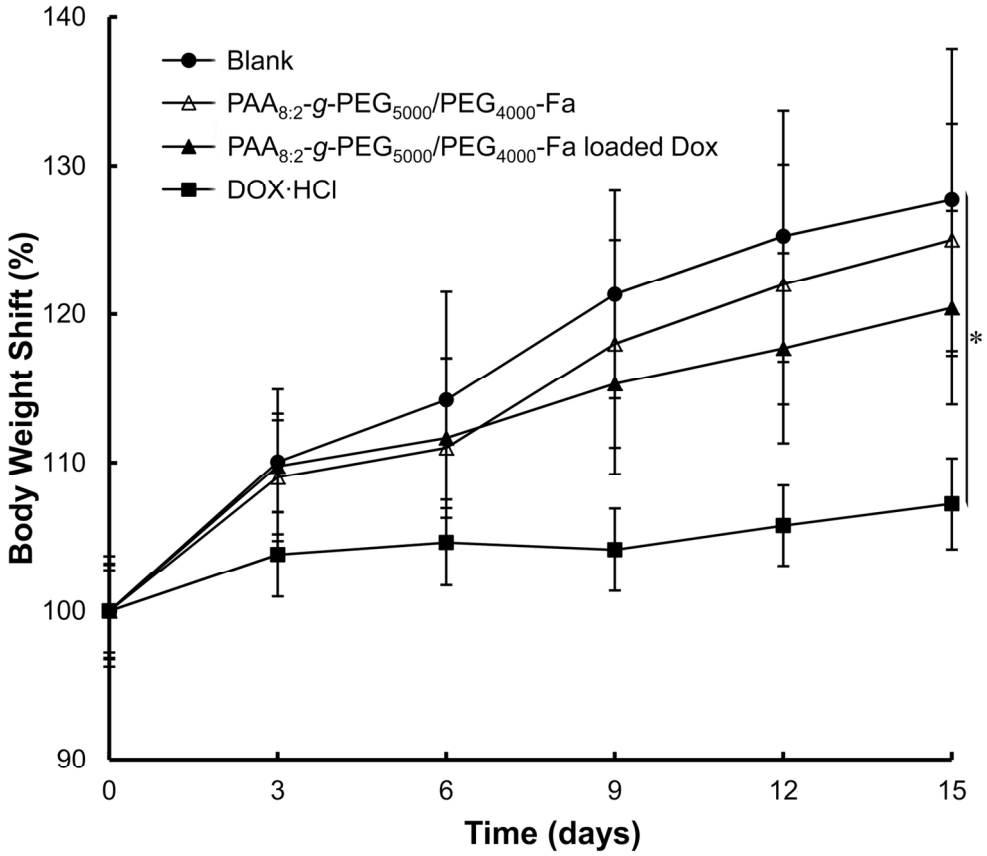

Figure 7
72x63mm (600 x 600 DPI)

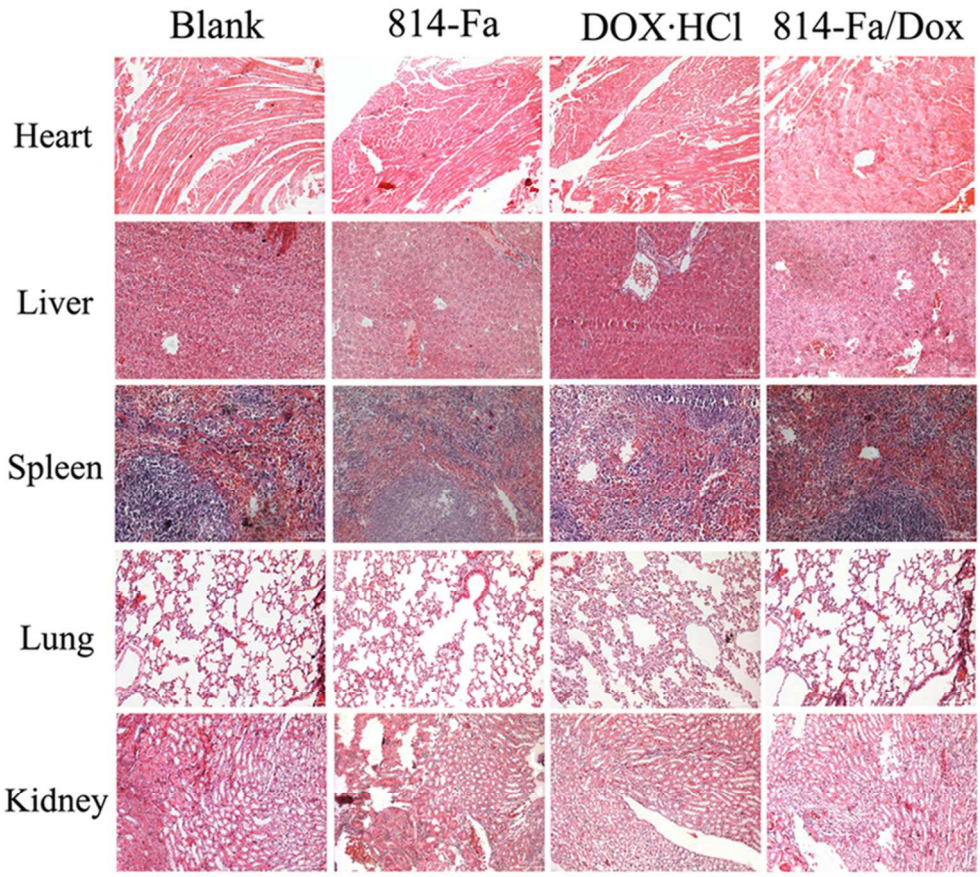

Figure 8
75x67mm (300 x 300 DPI)

Table 1 Synthesis and correlated characterization of amphiphilic polyamide amine-g-polyethylene glycol/polyethylene glycol conjugeted folate graft copolymers.

Series	PEA /EA[1]	PEG_{2000}:GE[2]/ PEG_{2000}-Fa:GE	PEG_{5000}:GE/ PEG_{4000}-Fa:GE	The Mol ratio value[2]	Size (nm)/PDI Dox-free	Dox-Fa	DLC (%)[3]	DLE (%)[4]
$PAA_{8:2}$-*g*-PEG_{2000}/PEG_{2000}-Fa	8:2	1:81%/1:77%		0.99	86.2 (0.156)	53.3 (0.158)	22.0	95.3
$PAA_{7:3}$-*g*-PEG_{2000}/2PEG_{2000}-Fa	7:3	1:87%/2:83%		1.34	55.1 (0.219)	35.7 (0.196)	20.7	89.7
$PAA_{7:3}$-*g*-2PEG_{2000}/PEG_{2000}-Fa	7:3	2:90%/1:80%		1.49	35.7 (0.203)	94.0 (0.121)	21.4	93.0
$PAA_{8:2}$-*g*-PEG_{5000}/PEG_{4000}-Fa	8:2		1:70%/1:63%	2.20	51.0 (0.332)	102 (0.136)	21.3	92.3
$PAA_{7:3}$-*g*-PEG_{5000}/2PEG_{4000}-Fa	7:3		1:74%/2:65%	2.90	53.5 (0.283)	106 (0.133)	21.7	94.3
$PAA_{7:3}$-*g*-2PEG_{5000}/PEG_{4000}-Fa	7:3		2:68%/1:57%	3.47	57.6 (0.328)	110 (0.139)	21.6	93.9

[1] PEA/EA: mol ratio=phenethylamine/ethanolamine

[2] GE: The conjugation efficiency of PEG and PEG-Fa

[3] The Mol ratio value: The molecular weight ratio value= hydrophilic segment (PEG)/hydrophobic segment (PAA and Folate)

[4] DLC: Drug loading Content

[5] DLE: Drug loading efficiency

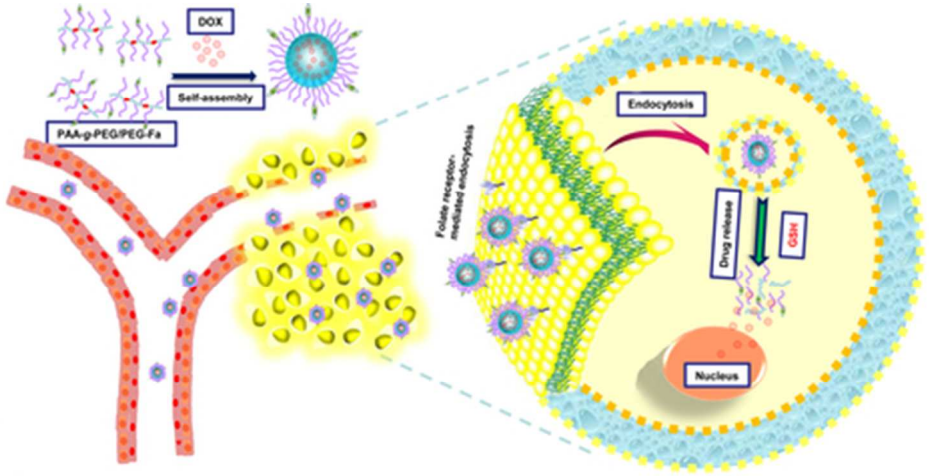

Scheme 2
39x19mm (300 x 300 DPI)

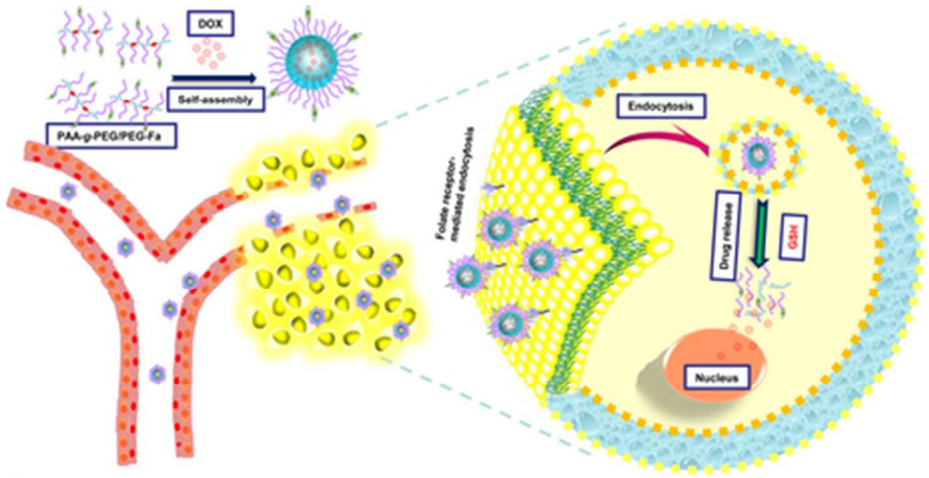

Graphical Abstract
39x19mm (300 x 300 DPI)